

CO₂ Corrosion of Mild Steel Exposed to CaCO₃-Saturated Aqueous Solutions

Hamed Mansoori,^{†,*} David Young,^{*} Bruce Brown,^{*} Srdjan Nešić,^{*} and Marc Singer^{*}

The behavior of CO₂ corrosion of mild steel was studied in a CaCO₃ saturated aqueous solution. The bulk water chemistry ([Fe²⁺], [Ca²⁺], and pH) was controlled and the mass transfer characteristics inherent to the experimental setup were well defined. A combination of weight loss and electrochemical techniques, as well as surface characterization tools, were used to assess the behavior of corrosion products over long-term experiments. Three corrosion periods were identified based on the analysis of the corrosion rates and Nyquist response values versus exposure time. Residual Fe₃C was the early corrosion product; however, Fe_xCa_yCO₃ (x + y = 1) precipitated within its pores over the course of experiments where a favorable local water chemistry was achieved, regardless of the bulk solution. Results show that the presence of Ca²⁺ did not jeopardize the final protectiveness of corrosion products.

KEY WORDS: CaCO₃, CO₂ corrosion, FeCO₃, Fe₃C, isostructurality

INTRODUCTION

Localized corrosion is typically influenced by the anionic species in electrolytes. However, localized corrosion has been also attributed to the inhomogeneity of the corrosion product layer in the presence of Ca²⁺, as a cationic species.¹ There are a number of contradictions in the open literature regarding the effect of Ca²⁺ on uniform and localized corrosion of mild steel in CO₂ environments.² This is often due to inadequate experimental setups and procedures, which fail to ensure consistent control of solution chemistry, such as pH and degree of CaCO₃ saturation. Aqueous speciation is one of the most influential parameters that governs both scaling and corrosion processes. The degree of aqueous saturation of CaCO₃ and FeCO₃ is a key parameter, even more important than individual ion concentrations, when studying the effect of Ca²⁺ ions on CO₂ corrosion. The precipitation kinetics of solid CaCO₃ and FeCO₃ are greatly influenced by the bulk saturation degree, as the main driving force, rather than individual ion concentrations.³ An electrolyte can have a high concentration of Ca²⁺ but still be undersaturated with respect to CaCO₃; bulk precipitation is not expected. Saturation degree depends on several environmental parameters, such as relevant ion concentration, pH, temperature, ionic strength, etc. Researchers often overlooked saturation degree, exclusively relying on ion concentrations as the core influencing parameter on CO₂ corrosion. pH is a critical parameter which has a considerable effect on corrosion rate as well as CaCO₃ and FeCO₃ precipitation rates. Many studies published on the effect of Ca²⁺ on CO₂ corrosion describe experiments where the initial and final solution pH values are not the same due to changes of water chemistry over the course of long-term experiments. In some cases, even the initial pH is not reported at all.⁴⁻⁵ The corrosion behavior and the formation of corrosion product layers and

scales are also influenced by mass transfer of key ions from/to the bulk solution and through surface layers.⁶ Mass transfer rate influences the concentration of the aqueous species near the corroding metal surface, which constitutes the active site for precipitation of metal carbonates. Consequently, the morphology and other properties of the surface layers can be considerably affected by mass transfer characteristics. Experimental data generated by a setup with well-defined mass transfer characteristics for studying the effect of Ca²⁺ on CO₂ corrosion ensures reproducibility.

In the research reported herein, methodologies were developed to overcome reported experimental difficulties and to obtain more reliable and repeatable results when studying the influence of Ca²⁺ on mild steel CO₂ corrosion mechanisms. The results were obtained in a system where the water chemistry of the test environment was tightly controlled over the course of the experiments, and where mass transfer characteristics were also well-defined. An extended version of this research letter is available for more detailed analysis and discussion.⁷ However, in the current manuscript, electrochemical impedance spectroscopy (EIS) data with relevant discussion are provided.

EXPERIMENTAL PROCEDURES

Figure 1 shows the experimental setup, equipped with fixed specimen holders and an impeller for generating uniform mass transfer characteristics across the specimen surfaces. These advancements were introduced to eliminate nonuniformity of flow and mass transfer experienced by unstable hanging specimens, as in the conventional glass cell setup used in a previous study.⁸ pH and [Fe²⁺] were controlled using H-form and Na-form ion-exchange resins, installed in two independently controlled flow loops attached to the glass cell. For more explanations about the effectiveness of the ion-exchange resins

Submitted for publication: July 1, 2019. Revised and accepted: September 8, 2019. Preprint available online: September 8, 2019, <https://doi.org/10.5006/3310>.
Recipient of first place in the Mars Fontana Corrosion Engineering category at CORROSION 2019, March 2019, Nashville, Tennessee.

[†] Corresponding author. E-mail: hm419213@ohio.edu.

* Institute for Corrosion and Multiphase Technology, Department of Chemical and Biomolecular Engineering, Ohio University, 342 West State Street, Athens, Ohio 45701.

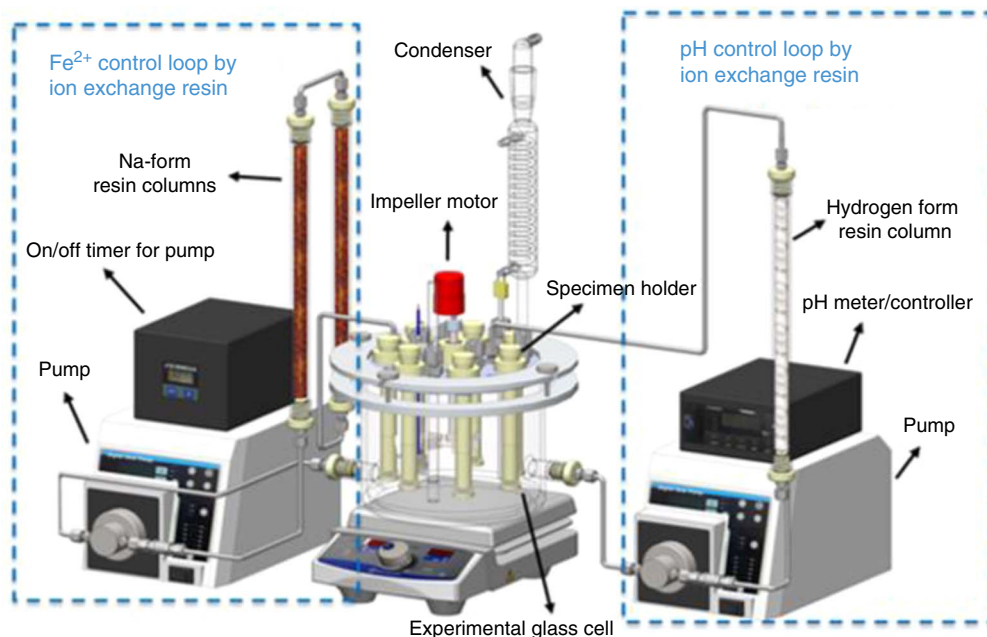


FIGURE 1. Schematic of the experimental setup equipped with fixed specimen holders and impeller, capable of controlling water chemistry.

Parameter	Description	
Specimen characteristics	UNS G10180 with ferritic-pearlitic structure, flat square geometry with a surface area of 1.5 cm ²	
Electrolyte	without Ca ²⁺	with 160 ppm Ca ²⁺
	1 wt% NaCl + NaHCO ₃ (ionic strength ~0.18 M)	1 wt% NaCl + CaCO ₃ (ionic strength ~0.18 M)
S _{CaCO₃}	0	Unity
S _{FeCO₃}	~10	
Mass transfer conditions	Equivalent to 0.5 m/s in a 0.1 m ID pipe (impeller: 20 rpm)	
Electrochemical techniques	LPR: potential range (±5 mV _{OCP}), scan rate (0.125 mV/s), B value (26 mV)	
	EIS: frequency range (10 K/mHz), DC voltage (zero vs. OCP), peak to peak amplitude (10 mV), sampling rate (8 points/decade)	

and their function in corrosion studies, please refer to the publication by Zhong, et al.⁹ The test solutions were kept saturated with respect to CaCO₃ over the course of 7 d experiments, corresponding to a stable [Ca²⁺] of ca. 160 ppm, by maintaining a deposit of solid CaCO₃ at the bottom of the glass cell. The [Ca²⁺] was measured at the beginning and end of experiments using inductively coupled plasma spectroscopy.

Defining the hydrodynamic and mass transfer characteristics of any new experimental corrosion setup is essential when studying the influence of flow on corrosion, and helps ensure reproducibility of the results.¹⁰ In the current experimental setup, the limiting current of a ferri-ferrocyanide coupled electrochemical reaction, Equation (1), was used to define the mass transfer coefficient.



The dependence of the Sherwood (Sh) number on the Reynolds (Re) and Schmidt (Sc) numbers was defined by performing multiple regressions to calculate the unknown

constants pertaining to the specific geometry of the glass cell setup with this impeller. The final empirical relationship is shown in Equation (2).

$$\text{Sh} = 1.47 \text{Re}^{0.63} \text{Sc}^{0.33} \quad (2)$$

Two series of corrosion experiments were performed (and repeated), one without Ca²⁺ ions (as a baseline) and one in a CaCO₃ saturated electrolyte. Other than that, both tests were conducted under the same experimental conditions as described in Table 1. The experiments were conducted at atmospheric pressure at 80°C and 0.53 bar (53 kPa) pCO₂. After addition of 1 wt% NaCl (to both electrolytes), CaCO₃ reagent (to the electrolyte containing Ca²⁺), or NaHCO₃ (to the baseline electrolyte), the electrolytes were deoxygenated by sparging with CO₂ for at least 2 h prior to the start of each experiment. At the same time, the solution was heated to 80°C, leading to a water vapor pressure of 0.47 bar (47 kPa) with the balance gas being CO₂. In these conditions, the autogenous initial pH for the electrolyte in the presence of the CaCO₃ reagent was pH 6.2 at

equilibrium. Therefore, to have similar testing environments, the pH of the baseline electrolyte (without any Ca^{2+}) was initially adjusted to 6.2 (using NaHCO_3). CO_2 gas was continuously bubbled into the solutions to maintain saturation with CO_2 during corrosion experiments. During the experiments, the pH was maintained at 6.2 ± 0.1 by the means of H-form ion-exchange resin (Dowex® G26[†]). The $[\text{Fe}^{2+}]$ was controlled to be no greater than 10 ppmw using a Na-form ion-exchange resin (Amberlite® IR 120[†]). The CaCO_3 -saturated solution initially contained 1.2 g/L powdered CaCO_3 reagent with 99% purity (ACROS Organics™[†]). This excess amount of CaCO_3 in the solution was calculated, using the solubility of CaCO_3 in the experimental condition presented in Table 1, to be three times higher than what was needed for the solution to remain saturated with respect to CaCO_3 over the course of the long-term experiments. Although a portion of the $[\text{Ca}^{2+}]$ in the electrolyte was potentially, and unwantedly, removed by the ion-exchange resins, the excess CaCO_3 reagent guaranteed that the solution remained saturated with respect to CaCO_3 with a stable $[\text{Ca}^{2+}]$ due to the relatively fast kinetics of CaCO_3 precipitation/dissolution.¹¹ A three-electrode configuration (including UNS G10180⁽¹⁾ material as working electrode, $\text{Ag}/\text{AgCl}_{\text{sat}}$ reference electrode, and Pt counter electrode) was used along with a Gamry Reference 600™[†] potentiostat to conduct electrochemical measurements.

RESULTS AND DISCUSSION

Figure 2 shows a comparison of corrosion rate (CR) obtained by linear polarization resistance (LPR) and open-circuit potential (OCP) for experiments with and without Ca^{2+} over time. A proportional constant of 26 mV (B value) was used for calculation of corrosion rate based on Stern-Geary theory.¹² It is understood that the value selected may be dependent on the specific testing conditions and may even change over the course of experiments. However, LPR data are used for trends rather than for obtaining values of corrosion rates which are measured more accurately by the weight loss method. Three corrosion periods can be identified in Figure 2 for experiments with and without Ca^{2+} :

1. Active corrosion (development of Fe_3C);
2. Nucleation/growth of surface layers (corrosion products);
3. Pseudo-passivation (further growth of corrosion products).

A longer active corrosion period was observed in the presence of 160 ppm Ca^{2+} . That may suggest that the presence of Ca^{2+} was interfering with the precipitation of FeCO_3 , slowing the processes of nucleation and/or growth. However, when the corrosion products are fully developed on the substrate, in the pseudo-passivation period, an identical corrosion rate is achieved with or without Ca^{2+} . Profilometry of the specimens after removal of corrosion products showed no localized corrosion for both electrolytes (baseline and CaCO_3 -saturated).

EIS measurements agreed with the LPR measurements in identifying the three corrosion periods. The impedance signatures for both series of experiments hold some similarities and differences. In order to show these characteristics, an example of EIS Nyquist data related to a CaCO_3 -saturated solution is presented and interpreted.

[†] Trade name.

⁽¹⁾ UNS numbers are listed in *Metals and Alloys in the Unified Numbering System*, published by the Society of Automotive Engineers (SAE International) and cosponsored by ASTM International.

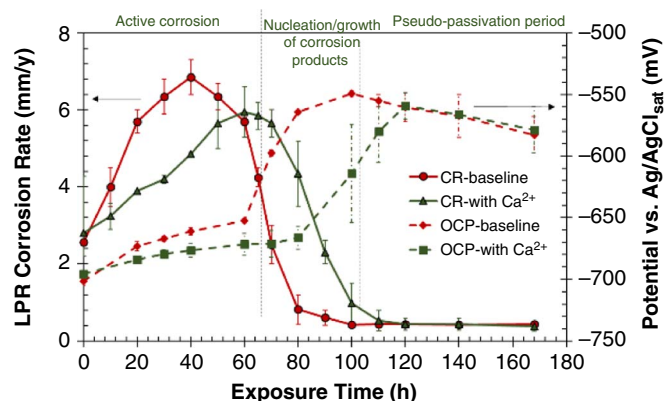


FIGURE 2. Comparison of corrosion rate and OCP over time for experiments with and without Ca^{2+} .

3.1 | Active Corrosion Period

Figure 3(a) shows the Nyquist plot evolution in this time period. Three time constants can be identified in this period. Two depressed capacitive semicircles and an inductive loop in the low-frequency (LF) range are obvious. The capacitive semicircle, in the high- (HF) to medium- (MF) frequency range, is related to the resistance of charge-transfer in the double-layer at the steel/solution interface and is inversely proportional to the corrosion rate.¹³ The second semicircle in the MF-LF range is related to development of a residual Fe_3C skeleton which remains due to the preferential corrosion of the α -Fe phase.¹⁴ The presence of an inductive loop in a CO_2 corrosion environment is usually associated with an adsorbed intermediate product.¹⁵ The magnitude of the inductive loop is decreasing with time as more conductive Fe_3C is exposed on the steel substrate, resulting in acceleration of hydrogen reduction. This is also reflected in the decrease of the overall impedance with time in this corrosion period. The inductive loop disappears after 74 h of exposure at the end of this period.

From 51 h to 74 h of exposure, the corrosion rates are near identical. This behavior could be explained by the balance between Fe_3C formation, which tends to increase the corrosion rate and the development of less aggressive water chemistry within the pores of Fe_3C where an increase of 2 to 3 pH units can be expected.

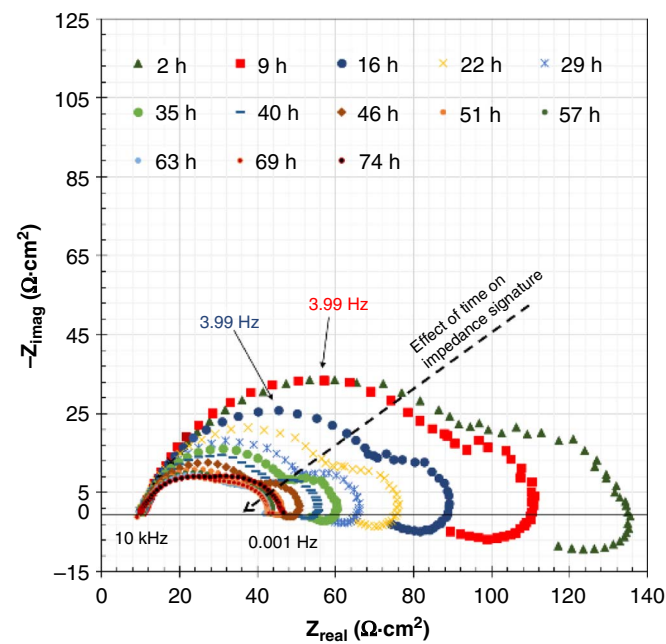
3.2 | Nucleation/Growth of Corrosion Product Period

This period roughly starts from 74 h of exposure with the nucleation of corrosion products happening within the pores of Fe_3C . Consequently, the corrosion rate decreases continuously as their further growth confers more protection against corrosion.

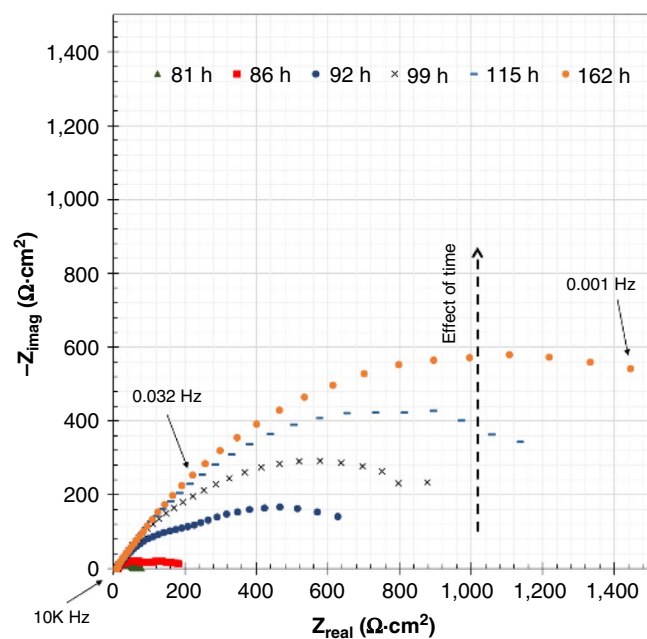
3.3 | Pseudo-Passivation Period

The pseudo-passivation period, which starts roughly after 99 h of exposure, is characterized by a low and steady corrosion rate and a higher OCP value (see Figure 2). The formation of a dense corrosion product layer is also achieved (supported by surface characterization, not shown in this manuscript⁷).

The Nyquist plots corresponding to the nucleation/growth and pseudo-passivation periods are provided in Figure 3(b). They show two incomplete semicircles with increasing diameters over time. This behavior is due to precipitation and growth of corrosion products.¹⁶ In addition, the inductive loops have disappeared completely.



(a)



(b)

FIGURE 3. Nyquist plots obtained for a UNS G10180 over time exposed to CaCO_3 -saturated solution (160 ppm Ca^{2+}) at 80°C , $p\text{CO}_2$ 0.53 bar, bulk solution pH 6.2, 0.18 M ionic strength, and 20 rpm: (a) active corrosion period and (b) nucleation/growth of corrosion products and pseudo-passivation periods.

CONCLUSIONS

> The presence of Ca^{2+} ions, while the solution is saturated with respect to CaCO_3 , did not jeopardize the protectiveness conferred by corrosion products in long-term CO_2 corrosion experiments nor initiated localized corrosion. Three corrosion periods were identified for corrosion of mild steel: active corrosion, nucleation/growth of corrosion products, and pseudo-passivation periods. Initially, residual Fe_3C constituted the main corrosion product. However, its pores became filled with $\text{Fe}_x\text{Ca}_y\text{CO}_3$ ($x + y = 1$) over the course of the experiments as a favorable water chemistry was achieved near the steel surface, regardless of the bulk solution.

ACKNOWLEDGMENTS

The authors would like to thank the following companies for their financial support: Anadarko, Baker Hughes, BP, Chevron, CNOOC, ConocoPhillips, DNV GL, ExxonMobil, M-I SWACO (Schlumberger), Multi-Chem (Halliburton), Occidental Oil Company, PTT, Saudi Aramco, SINOPEC (China Petroleum), and TOTAL.

References

1. S.N. Esmaeely, D. Young, B. Brown, S. Nešić, *Corrosion* 73 (2017): p. 238-246.
2. H. Mansoori, D. Young, B. Brown, M. Singer, *J. Nat. Gas Sci. Eng.* 59 (2018): p. 287-296.
3. T.H. Chong, R. Sheikholeslami, *Chem. Eng. Sci.* 56 (2001): p. 5391-5400.
4. C. Ding, K. Gao, C. Chen, *Int. J. Miner. Metall. Mater.* 16 (2009): p. 661-666.
5. G.X. Zhao, L. Jian-Ping, H. Shi-Ming, L.U. Xiang-Hong, *J. Iron Steel Res. Int.* 12 (2005): p. 38-42.
6. S. Nešić, *Energy Fuels* 26 (2012): p. 4098-4111.
7. H. Mansoori, D. Young, B. Brown, S. Nešić, M. Singer, *Corros. Sci.* 158 (2019): article id 108078.
8. S.N. Esmaeely, Y.-S. Choi, D. Young, S. Nešić, *Corrosion* 69 (2013): p. 912-920.
9. X. Zhong, B. Brown, W. Li, S. Nešić, M. Singer, "How to Maintain a Stable Solution Chemistry when Simulating CO_2 Corrosion in a Small Volume Laboratory System," CORROSION 2016, paper no. 7780 (Houston, TX: NACE International, 2016).
10. D.C. Silverman, *Corrosion* 60 (2004): p. 1003-1023.
11. N. Spanos, P.G. Koutsoukos, *J. Phys. Chem. B* 102 (1998): p. 6679-6684.
12. M. Stern, A.L. Geary, *J. Electrochem. Soc.* 104 (1957): p. 56-63.
13. Z. Zeng, R.S. Lillard, H. Cong, *Corrosion* 72 (2016): p. 805-823.
14. F. Farelas, M. Galicia, B. Brown, S. Nešić, H. Castaneda, *Corros. Sci.* 52 (2010): p. 509-517.
15. G.A. Zhang, Y.F. Cheng, *Corros. Sci.* 51 (2009): p. 87-94.
16. J.L. Mora-Mendoza, S. Turgoose, *Corros. Sci.* 44 (2002): p. 1223-1246.